

# Double Fourier Integral Analysis based Convolutional Neural Network Regression for High-Frequency Energy Disaggregation

Pascal A. Schirmer and Iosif Mporas

**Abstract**—Non-Intrusive Load Monitoring aims to extract the energy consumption of individual electrical appliances through disaggregation of the total power load measured by a single smart-meter. In this article we introduce Double Fourier Integral Analysis in the Non-Intrusive Load Monitoring task in order to provide more distinct feature descriptions compared to current or voltage spectrograms. Specifically, the high-frequency aggregated current and voltage signals are transformed into two-dimensional unit cells as calculated by Double Fourier Integral Analysis and used as input to a Convolutional Neural Network for regression. The performance of the proposed methodology was evaluated in the publicly available UK-DALE dataset. The proposed approach improves the estimation accuracy by 7.2% when compared to the baseline energy disaggregation setup using current and voltage spectrograms.

**Index Terms**—Energy Disaggregation, Non-Intrusive Load Monitoring (NILM), Spectrogram, Double Fourier Integral Analysis (DFIA).

## I. INTRODUCTION

GLOBAL average temperatures are rising due to the increasing amount of greenhouse gas emissions causing natural disasters and having negative impact on nature and humankind alike. As households are responsible for approximately 40% of the total consumed energy worldwide and thus for the corresponding  $CO_2$  emissions, optimization of households energy consumption is a very promising direction in order to reduce total energy consumption [1]. Specifically, approaches based on energy prediction [2], [3], energy management [4], local storages [5] as well as detailed optimizations, e.g. management of high power devices [6], have been proposed to address this issue. Moreover, studies estimate that 5%-20% of households' consumed energy could be saved by changing consumers' behaviour and improving the existing poor operational strategies [7], [8]. To address these challenges detailed analysis of energy consumption on device level is necessary [9].

The analysis of energy on device level is performed through energy disaggregation, i.e. the extraction of energy consumption on appliance level based on one or multiple energy

consumption measurement sensors called smart-meters [10]. When using only one sensor at the main inlet of a household, thus measuring only the aggregated consumption, the energy disaggregation task is referred to as Non-Intrusive-Load-Monitoring (NILM) [11], in contrast to Intrusive-Load-Monitoring (ILM) where multiple sensors are used, usually one per device. The goal of NILM is to estimate the energy consumption of each device using only the measured aggregated signal, thus NILM is considered a source separation problem.

Several NILM methodologies have been proposed in the literature, briefly been classified in approaches with or without source separation algorithms. Methods without source separation are using machine learning algorithms for regression like Convolutional Neural Networks (CNNs) [12], [13], Recurrent Neural Networks (RNNs) [14], Long Short Time Memory (LSTM) [15], [16], as well as Hidden Markov Models (HMMs) and their variants [17], [18]. Combinations of machine learning algorithms for fusion of information [19] and modelling of temporal dynamics [20] have also been proposed. As regards methods using source separation algorithms they are based on non-negative matrix/tensor factorization [21]–[23], integer non-linear programming [24] and sparse-coding [25], [26] using additional constraints (e.g. sum-to-one or cross-entropy) on the optimization problem [27], [28]. Furthermore, approaches based on pattern matching and graph signal processing have also been proven to work well [29], [30]. Considering features, most of the NILM methods use only active power [31], others also use reactive power, raw current/voltage and their harmonics [32], [33], while some methods calculate new features for the NILM task, e.g. based on fractional calculus [14]. Additionally methods for reduction of feature dimensionality have been presented [34].

Most of the proposed NILM methods use Low Frequency measurements (LF), which are in the range of one up to ten samples per second, in order to meet the limitations of the usually low-cost hardware (CPU and RAM) of smart-meters, as well as the limitations of the communication channel bandwidth for the transmission of the acquired samples [35]. In the last two decades LF NILM methodologies' performance has been improved significantly especially for devices with steady-state behaviour, i.e. devices with discrete operational states and time invariant signatures (e.g. fridges), in low 'noise' conditions, i.e. identifying high power devices from the aggregated signal with relatively low energy consumption from background/unknown loads [35], [36]. The main drawback of

P.A. Schirmer and I. Mporas are with the School of Physics, Engineering and Computer Science, Intelligent Systems Group CIS, University of Hertfordshire, Hatfield, UK, AL10 9AB England e-mail: {p.schirmer,i.mporas}@herts.ac.uk.

Copyright 2020 IEEE. Personal use of this material is permitted. Permission from IEEE must be obtained for all other uses, in any current or future media, including reprinting/republishing this material for advertising or promotional purposes, creating new collective works, for resale or redistribution to servers or lists, or reuse of any copyrighted component of this work in other works.

LF NILM methods is that they are not capable of accurately capturing the power consumption signature characteristics of non-steady state devices as well as devices with strong non-linear behaviour during their start-up (e.g. induction motors). For these devices High Frequency (HF) analysis is needed as shown in [37]–[39]. Furthermore, improvements of HF NILM have been shown for unsupervised and transfer-learning approaches in [40], [41] and [42], respectively. Moreover, source separation based NILM using HF data has been shown to improve energy disaggregation performance as well [21]. In detail, the approach presented in [21] uses additional smoothness constraints on the matrix factorization problem, while the approach in [43] combines HF binary matrix factorization with an additional neural network to improve online estimation of appliances’ working routines.

HF based NILM methods found in the bibliography are based either on spectrogram analysis [44], [45] or on current-voltage trajectories [42], [46]. In detail, selection of odd harmonic current vectors for identification of variable power loads and power electronics has been presented in [47], [48]. Furthermore, a frequency invariant transformation for periodic current signals has been presented in [49] converting uncorrelated samples to multiples of the grid frequency. Moreover, the approach in [50] uses odd current harmonics in combination with a transient event detection stage and utilizes a bipartite graph matching problem for disaggregation. Additionally, a high-frequency spectrogram approach is presented in [44], which considers next to current spectrograms also voltage fluctuations. Specifically, the utilization of voltage and current harmonics has been discussed in [51], while high-frequency voltage signatures have been utilized in the form of voltage and current trajectories in [42]. To the best of the authors knowledge specific consideration of voltage harmonics and especially odd and even order harmonics has not been carried out within the context of NILM.

In this article Double Fourier Integral Analysis (DFIA), which is an established method for analytical transient signal analysis of power electronics adapted by Bowes and Bird [52], [53] and was originally developed for communication systems by Bennet and Black [54], [55], is used for HF NILM. DFIA was used in order to calculate enhanced frequency representations including baseband, sideband and carrier harmonics of current and voltage using two-dimensional Fourier transform, providing more accurate representation of transient events. The proposed method was evaluated on the UK-DALE dataset to disaggregate eight out of 52 electrical appliances, for the purpose of direct comparison with previous publications. In detail, the approach in [44] was used as it is a high-frequency CNN based approach similar to the proposed architecture. Furthermore, four low-frequency architectures have been chosen for additional comparison, namely [56], [57] in which the UK-DALE dataset was initially evaluated, the approach in [58] utilizing a sequence-to-point learning based approach, as well as the approach in [59] utilizing dictionary learning thus a source-separation based approach.

The contribution of the paper is twofold. First, DFIA is adapted to the NILM task in order to provide more distinct HF features based on the decomposition of harmonics into funda-

mental, base-band, carrier and sideband harmonics considering both odd and even current and voltage harmonics. Second, the advantageous performance of using DFIA signatures as features for the NILM task over using spectrogram based approaches for NILM is evaluated in terms of performance as well as robustness against outliers and noise. The remainder of this paper is organized as follows: In Section II an introduction to DFIA of energy consumption signals is given. In Section III the proposed method is presented. In Section IV the experimental setup is described and in Section V the evaluation results are presented. Finally, discussion is provided in Section VI and the article is concluded in Section VII.

## II. DOUBLE FOURIER INTEGRAL ANALYSIS OF ENERGY CONSUMPTION SIGNALS

In order to analyze signals with transient components, e.g. with frequency content varying in time, signals are segmented to frames (short-time analysis) and spectrograms are traditionally used for time-frequency representation of each frame. A frequency-frequency representation using DFIA is introduced as an alternative to frame spectrograms for HF NILM. The mathematical formulation of frame spectrograms and DFIA for energy disaggregation is given below.

### A. Spectrogram Analysis

Let  $i_{agg}(t)$  be the discrete-time signal after A/D conversion with sampling period  $T_s$  of the aggregated current, continuously measured by a smart meter with  $t \in \mathbb{N}_0$ , i.e. starting at time  $t = 0$ . The signal is decomposed into consecutive segments (frames) of length  $W$  samples each, to perform short-time analysis (successive frames might be overlapping in time or not). Given an arbitrary frame  $i_{agg}^\tau$  of  $i_{agg}$ , with  $i_{agg}^\tau = [i(t_0), i(t_0 + 1), \dots, i(t_0 + W - 1)]$  and  $t_0$  being the first sample of the  $\tau$ -th frame, the spectrogram of the frame is realized as a two-dimensional matrix  $S$ :

$$S(i_{agg}^\tau) = [|\tilde{i}_{agg}^{\tau,1}|, |\tilde{i}_{agg}^{\tau,2}|, \dots, |\tilde{i}_{agg}^{\tau,\lambda}|, \dots, |\tilde{i}_{agg}^{\tau,\Lambda}|] \quad (1)$$

with columns  $\tilde{i}_{agg}^{\tau,\lambda} \in \mathbb{C}^{N \times 1}$  being the  $N$ -point Discrete Fourier Transforms (DFT) of blocks (subframes) of  $N$  samples:

$$\tilde{i}_{agg}^{\tau,\lambda} = \sum_{n=0}^{N-1} i_{agg}^{\tau,\lambda}(n) \cdot e^{-j \frac{2\pi k}{N} n} \quad (2)$$

with  $0 \leq k \leq N - 1$ ,  $i_{agg}^{\tau,\lambda} \in \mathbb{R}^{N \times 1}$  being the  $\lambda$ -th subframe and  $j$  being the complex operator. For the last subframe  $\lambda = \Lambda$  either zero padding is applied to fill in the missing samples up to  $N$ , or these last samples are ignored resulting in one less subframe. Therefore, the spectrogram of each frame  $\tau$  of the aggregated current signal  $i_{agg}$  will be  $S(i_{agg}^\tau) \in \mathbb{R}^{N \times \Lambda}$ , which is a time ( $\Lambda$  columns) vs. frequency ( $N$  rows) representation of the frame  $i_{agg}^\tau$ . Similarly, the spectrogram of frame  $v_{agg}^\tau$  of the aggregated voltage signal  $v_{agg}$  will be  $S(v_{agg}^\tau) \in \mathbb{R}^{N \times \Lambda}$ .

It is noted that the spectrogram matrices,  $S(i_{agg}^\tau)$  and  $S(v_{agg}^\tau)$ , generally consist of complex number values (as a result of DFT), however when applied as input to a classifier for energy disaggregation usually the magnitude values of the

spectrogram matrices are used [44]. This is due to the fact that for electrical signals only the phase-shift between current and voltage has a physical meaning. In detail, the phase-shift between the fundamental component of the voltage and the fundamental component of the current determines the ratio of active and reactive power. Moreover, the current harmonics and their phase-shift with respect to the voltage harmonics determine the distortion reactive power [60]. Conversely, phase-shifts between the fundamental current and its harmonics do not carry any physical meaning.

### B. Double Fourier Integral Analysis

While in spectrogram analysis one discrete-time signal is considered, DFIA assumes two different time-dependent variables [61]. Let  $i_{agg}(t)$  and  $v_{agg}(t)$  be the aggregated current and the aggregated voltage signals, continuously measured by a smart meter, as described in Section II-A. The two signals are periodic towards the period of the power line frequency  $f_{el} = \omega_{el}/2\pi$  with  $\omega_{el}$  being the circular frequency of the grid and are time-aligned (time synchronous acquisition and in parallel A/D conversion), thus when each signal is segmented to frames of length  $W$  samples for any arbitrary frame  $i_{agg}^\tau$  of  $i_{agg}$ , with  $i_{agg}^\tau = [i(t_0), i(t_0+1), \dots, i(t_0+W-1)]$ , there is also a frame  $v_{agg}^\tau$  of  $v_{agg}$ , with  $v_{agg}^\tau = [v(t_0), v(t_0+1), \dots, v(t_0+W-1)]$ , with  $t_0$  being the first sample of  $i_{agg}$  and  $v_{agg}$  respectively. In DFIA an output function  $f(\cdot)$  is defined [24] by the cyclically varying signals  $i_{agg}^\tau$  and  $v_{agg}^\tau$ , i.e.  $f(v_{agg}^\tau, i_{agg}^\tau)$ , which in our case is the instantaneous power  $p_{x,y}^\tau = i_{agg}^\tau(x) \cdot v_{agg}^\tau(y)$  with  $1 \leq x, y \leq W$  and  $P^\tau \in \mathbb{R}^{W \times W}$  being the instantaneous power 2-d representation on a V-I plane for the  $\tau$ -th frame as illustrated in Fig. 1.

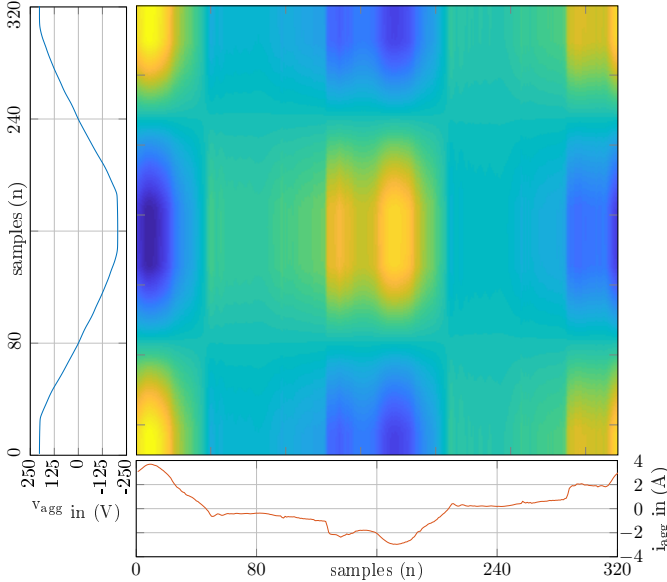


Fig. 1. Instantaneous power 2-d representation for one subframe (one electrical cycle) of aggregated current and voltage.

As shown in Fig. 1 each V-I instantaneous power frame,  $P^\tau$ , contains the current and voltage trajectories in  $x/y$  directions. From Fourier series theory [61] any time varying periodic function of two variables, i.e.  $f(i_{agg}, v_{agg})$ , can be written

as a sum of harmonic components, as introduced as part of the DFIA in communication systems [54] as well as in power electronics [53]. In this article, the description from [62] is used, i.e.

$$\begin{aligned}
 f(i_{agg}, v_{agg}) = & \underbrace{\frac{A_{00}}{2}}_{\text{DC-Offset}} \quad (3) \\
 & + \underbrace{\sum_{l=1}^{\infty} [A_{0l} \cdot \cos(li_{agg}) + B_{0l} \cdot \sin(li_{agg})]}_{\text{fundamental component \& baseband harmonics}} \\
 & + \underbrace{\sum_{k=1}^{\infty} [A_{k0} \cdot \cos(kv_{agg}) + B_{k0} \cdot \sin(kv_{agg})]}_{\text{carrier harmonics}} \\
 & + \underbrace{\sum_{k=1}^{\infty} \sum_{l=-\infty}^{\infty} [A_{kl} \cos(kv_{agg} + li_{agg}) + B_{kl} \sin(kv_{agg} + li_{agg})]}_{\text{sideband harmonics}}
 \end{aligned}$$

where  $k$  is the index variable for the voltage and  $l$  is the index variable for the current. As can be seen Eq. 3 can be decomposed into four terms: DC-component, fundamental component and baseband harmonics, carrier harmonics and sideband harmonics. The DC-component describes the transferred DC power ( $k, l = 0$ ). The fundamental component and baseband harmonics are the AC power ( $l = 1$ ) and the low frequency current harmonics ( $l > 1$ ). The carrier harmonics (in our case voltage is considered as a carrier, as it is fixed by the grid, similar as a modulation wave) for voltage distortions ( $k \geq 1$ ). The sideband harmonics, which are ensembles of sums and differences of current and voltage waveforms, and can be found at frequencies  $f = f_{el} \cdot k + f_{el} \cdot l$ .

The overall harmonic current and voltage fingerprint of a frame  $P^\tau$  is described by the coefficients  $A_{kl}$  and  $B_{kl}$ , in contrast to the spectrograms  $S(i_{agg}^\tau)$  and  $S(v_{agg}^\tau)$ , which contain only fundamental components and baseband harmonics of the current or the voltage signal only. For the purpose of energy disaggregation, the double Fourier transform is calculated for each frame  $P^\tau$ , i.e.

$$F_{k,l}^\tau = A_{k,l} + jB_{k,l} = \frac{1}{W^2} \sum_{x=1}^W \sum_{y=0}^W p_{x,y} \cdot e^{-j2\pi(\frac{k}{W}x + \frac{l}{W}y)} \quad (4)$$

with  $1 \leq k < K$  and  $1 \leq l < L$  being index variables. The magnitude and/or phase of each unit cell  $F_{k,l}^\tau \in \mathbb{C}^{W \times W}$  are then used as input to a machine learning model for classification or regression. The coefficients  $A_{k,l}$  and  $B_{k,l}$  represent the magnitude of the harmonics. The two-dimensional magnitudes  $H_{k,l}$  and phase angles  $\Phi_{k,l}$  of the harmonic components can then be written using the coefficients  $A_{k,l}$  and  $jB_{k,l}$ :

$$H_{k,l} = \text{abs}(F_{k,l}) = |A_{k,l} + jB_{k,l}| = \sqrt{A_{k,l}^2 + B_{k,l}^2} \quad (5)$$

$$\Phi_{k,l} = \text{arctan2}\left(\frac{A_{k,l}}{B_{k,l}}\right) \quad (6)$$

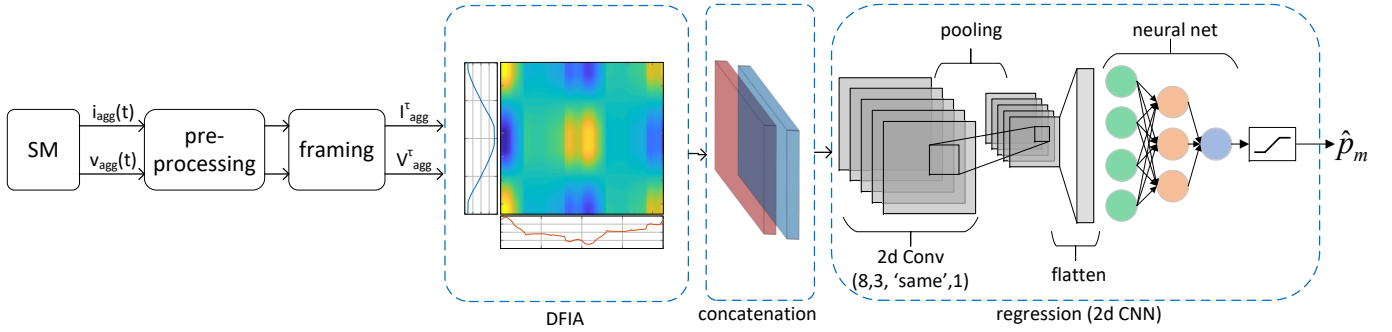


Fig. 2. Proposed high frequency CNN architecture utilizing double Fourier integral analysis, with one CNN model trained for each device  $m$ .

with  $H \in \mathbb{R}^{W \times W}$  and  $\Phi \in \mathbb{R}^{W \times W}$ .

The DFIA magnitude of the two-dimensional instantaneous power representation of Fig. 1 is illustrated in Fig. 2.

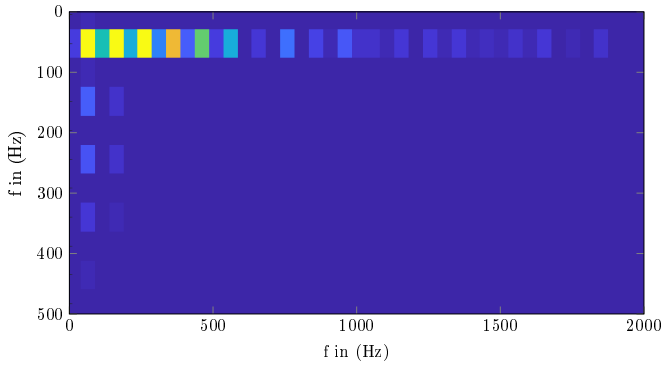


Fig. 3. DFIA magnitude with the y-axis being the voltage direction and the x-axis being the current direction

Specifically, the current/voltage harmonics (baseband/carrier harmonics) can be found along the  $x/y$ -axis with the fundamental component at  $k, l = 1$  and  $f_{el}=50$  Hz and the DC component at  $k, l = 0$  and  $f_{el}=0$  Hz, while odd order harmonics can be found in both current and voltage direction for  $k, l = \{3, 5, 7, \dots\}$  thus  $f_{k,l} = \{150Hz, 250Hz, 350Hz, \dots\}$ . Furthermore, it can be seen that harmonics are decaying significantly faster in voltage direction (y-axis) than in current direction (x-axis), accurately capturing the time-domain behaviour as illustrated in Fig. 1. Moreover, sideband harmonics can be seen, especially in the current direction, appearing at  $f = f_{el} \cdot k + f_{el} \cdot l$ , e.g. for  $k = 1$  and  $l = \{1, 3, 5, \dots\}$  at  $f_{1,l} = \{100Hz, 200Hz, 300Hz, \dots\}$ .

### III. NILM USING DOUBLE FOURIER INTEGRAL ANALYSIS

In the NILM task the energy consumption measurements of one sensor are disaggregated on device level, within time windows (frames). Specifically, for a set of  $M$  devices, consisting of  $M - 1$  known devices and one ghost device (sum of all unknown devices), each consuming power  $p_m$ , with  $1 \leq m \leq M$ , the aggregated power  $p_{agg}$  measured by the sensor will be:

$$p_{agg} = f(p_1, p_2, \dots, p_{M-1}, g) = \sum_{m=1}^{M-1} p_m + g = \sum_{m=1}^M p_m \quad (7)$$

where  $g = p_M$  is a ‘ghost’ power consumption (noise) usually consumed by one or more unknown devices with  $f(\cdot)$  being the aggregation function. In NILM the goal is to find estimations,  $\hat{p}_m$  and  $\hat{g} = \hat{p}_M$ , of the power consumption of each device  $m$  using a disaggregation function  $f^{-1}(\cdot)$ , i.e.

$$\hat{P} = \{\hat{p}_1, \hat{p}_2, \dots, \hat{p}_{M-1}, \hat{g}\} = f^{-1}(p_{agg}) \quad (8)$$

where  $\hat{P}$  is a set of all predicted appliances, i.e.  $\hat{P} = \{\hat{p}_1, \hat{p}_2, \dots, \hat{p}_{M-1}, \hat{g}\}$  and  $P \in \mathbb{R}^M$ . The baseline approach in HF NILM [44] and in HF load classification is relying on classification/regression of frame spectrograms of the current  $S(i_{agg}^\tau)$  and/or the voltage  $S(v_{agg}^\tau)$ , i.e.

$$\hat{P} = \{\hat{p}_1, \hat{p}_2, \dots, \hat{p}_{M-1}, \hat{g}\} = r(S(i_{agg}^\tau), S(v_{agg}^\tau)) \quad (9)$$

where  $r(\cdot)$  is a regression model which approximates the inverse aggregation function  $f^{-1}(\cdot)$ , i.e.  $r(\cdot) \approx f^{-1}(\cdot)$ . In the proposed approach for each of the  $M$  devices one regression model is trained with the corresponding outputs being limited up to the overall power, i.e.  $\hat{p}_m < p_{agg}$ . In the proposed approach the devices’ power consumption estimation is performed using the magnitude  $H$  and phase angle  $\Phi$  of the instantaneous power matrices extracted per frame from the DFIA as described in Section II-B, i.e.

$$\hat{P} = \{\hat{p}_1, \hat{p}_2, \dots, \hat{p}_{M-1}, \hat{g}\} = r(H, \Phi) \quad (10)$$

The block diagram of the proposed HF NILM architecture is illustrated in Fig. 3. In detail, the architecture illustrated in Fig. 3 consists of pre-processing, framing, extraction of frames’ instantaneous power matrix and DFIA, concatenation of magnitude and phase matrices to  $N \times \Lambda \times 2$  arrays per frame, and one CNN regression model for each target device  $m$  to estimate the corresponding power consumption  $\hat{p}_m$ .

### IV. EXPERIMENTAL SETUP

The NILM architecture based on double Fourier integral analysis described in Section III was evaluated using the datasets, features and regression algorithm presented below.

### A. Datasets

Four datasets with HF measurements exist [63]–[66], to the best of our knowledge, with REDD [63] and UK-DALE [64] being used in regression based NILM tasks. Previous approaches on HF NILM have been evaluated on houses 1 and 3 of REDD [63] dataset and houses 1, 2 and 5 of UK-DALE [64] dataset, as for these houses continuous HF aggregated measurements have been recorded. As the proposed approach relies on Fourier analysis, UK-DALE has been selected for its evaluation, as REDD has HF measurements only from time intervals in which high amplitude change of line current or voltage appears. UK-DALE aggregated voltage and current measurements have been recorded at sampling frequency equal to 16 kHz, while the corresponding time-aligned signals per device have been recorded at sampling frequency equal to 1 Hz. House one of the UK-DALE was selected as it contains significantly more appliances (52 appliances) than the other houses ( $\sim 20$  appliances), thus offering realistic conditions of a household appliances operational routine. For our evaluation the 1<sup>st</sup>-7<sup>th</sup> December 2014 (7 days) of the HF data was chosen (32 GB compressed stored data size) as it contains simultaneous activity of up to twelve appliances. In detail, to efficiently train the proposed high-frequency CNN architecture for each of the eight devices, six days of the high-frequency aggregated data (input) were used to train a CNN model for each devices using its low frequency active power as ground-truth signal (output). Afterwards, testing was performed on the remaining day of the data.

In order for an disaggregation approach to be efficient it should disaggregate a high proportion of the total consumed energy in the household [63]. Therefore, the five appliances with the highest energy consumption were chosen for evaluation of disaggregation performance, namely the boiler (BO), the washing machine (WM), the kitchen lights (KL), the fridge (FR) and the total lightning circuit (TL). It must be noted that in the proposed appliance selection lighting has an disproportional high share of the total energy, which is due to the selected time period (December). Moreover, to compare with different previously proposed architecture [44], [56]–[59] we extended the selected appliances by including another three devices, namely the dishwasher (DW), the microwave (MW) and the kettle (KT), thus resulting in eight devices in total.

### B. Preprocessing and Parametrization

During pre-processing each of the aggregated voltage and current signals was frame blocked in frames of  $W=16000$  samples, thus for each frame of 16000 samples of HF data there is one sample of the ground-truth appliance signals. Moreover, for calculating the current and voltage spectrograms the frames were split into  $\Lambda$  subframes with length  $\frac{16000Hz}{50Hz}=320$  samples, thus one electrical period, with overlap between successive subframes equal to 50% (i.e. 180 samples).

For the regression stage a two-dimensional Convolutional Neural Network (CNN) was used, as in [44]. In detail, the CNN regression model takes as input the two-dimensional features as calculated by the spectrogram analysis or DFIA and learns the free parameters of the network using low-frequency

active power signatures of the appliances (output). One CNN regression model per device is used. Furthermore, the free parameters of the CNN, namely the number of filters and the kernel size for each of the convolutional layers, as well as the pooling size and the number of neurons in the dense layer were optimized through grid search on a bootstrap dataset (12h of operation including on and off periods for each device). The optimal number of convolutional layers is three, while the grid search for finding the optimal number of filters and kernel size is shown in Table I.

TABLE I  
PARAMETER OPTIMIZATION OF CNN MODEL IN TERMS OF  $E_{ACC}$  WITH DIFFERENT KERNEL SIZE AND NUMBER OF FILTERS.

Kernel	Number of filters				
	2	4	8	16	32
1	61.3%	79.5%	76.4%	73.9%	73.4%
2	63.6%	70.2%	80.5%	74.0%	79.4%
3	79.8%	76.4%	<b>82.3%</b>	67.3%	77.8%
4	68.1%	67.8%	64.7%	61.1%	76.1%
5	71.0%	61.0%	53.2%	60.4%	63.7%

As illustrated in Table I the optimal number of filters is eight and the optimal kernel size is three. The optimal CNN structure used for NILM is tabulated in Table II.

TABLE II  
OPTIMAL HF CNN STRUCTURE FOR NILM

Nr.	Layer	Nr.	Layer
1	Input	9	BatchNormalization
2	Conv2d(8,3,'same',1)	10	Relu
3	BatchNormalization	11	Maxpool(4)
4	Relu	12	Flatten
5	Conv2d(8,3,'same',1)	13	Dense(256)
6	BatchNormalization	14	Relu
7	Relu	15	Dense(1)
8	Conv2d(8,3,'same',1)	16	Linear activation

The pool size of the maxpool layer and the number of neurons in the dense layer were optimized after grid search on the same bootstrap dataset as for the parametrization of the convolutional layers and were found to be four for the max-pooling layer and 256 neurons for the dense layer. All convolutional layers have the same padding and stride sizes all equal to one.

### C. Experimental Protocols

Six experimental protocols were designed, three with respect to the use of current and voltage spectrograms (baseline approach) and three based on the proposed DFIA. To assure fair comparison between the approaches the dimensionality of DFIA based magnitude and phase being originally  $W \times W$  was resized in order to match the dimensionality of the corresponding spectrograms  $N \times \Lambda$ . In detail, to keep the best feature representation during the size reduction of the two-dimensional signatures the number of voltage harmonics ( $\Lambda$ ) was stronger reduced than the number of current harmonics

( $N$ ). This is due to the fact, that the voltage fluctuation is usually significantly smaller than the current fluctuation and thus carries less information [44]. The six protocols are tabulated in Table III.

TABLE III  
SIX EVALUATED EXPERIMENTAL PROTOCOLS INCLUDING THEIR FEATURES AND DIMENSIONALITY

Protocol	Features	Dimensionality
I	Current Spectrogram	$\tilde{I}_{agg} \in \mathbb{R}^{N \times \Delta}$
V	Voltages Spectrogram	$\tilde{V}_{agg} \in \mathbb{R}^{N \times \Delta}$
V-I	Current/Voltage Spectrogram	$\tilde{VI}_{agg} \in \mathbb{R}^{2 \times N \times \Delta}$
$DF_H$	Magnitudes DFIA	$DF_H \in \mathbb{R}^{N \times \Delta}$
$DF_\Phi$	Phases of DFIA	$DF_\Phi \in \mathbb{R}^{N \times \Delta}$
$DF_{H-\Phi}$	Magnitudes/Phases DFIA	$DF_{H-\Phi} \in \mathbb{R}^{2 \times N \times \Delta}$

### V. EXPERIMENTAL RESULTS

The DFIA approach presented in Section III was evaluated according to the experimental setup described in Section IV. The performance was evaluated in terms of estimation accuracy on device level ( $E_{ACC}^m$ ) and on average ( $E_{ACC}$ ), as proposed in [63], taking into account the estimated power  $\hat{p}_m$  where  $T$  is the total number of disaggregated frames and  $m$  is the device number respectively.

$$E_{ACC} = 1 - \frac{\sum_{m=1}^M \sum_{\tau=1}^T |\hat{p}_m^\tau - p_m^\tau|}{2 \sum_{m=1}^M \sum_{\tau=1}^T |p_m^\tau|} \quad (11)$$

$$E_{ACC}^m = 1 - \frac{\sum_{\tau=1}^T |\hat{p}_m^\tau - p_m^\tau|}{2 \sum_{\tau=1}^T |p_m^\tau|} \quad (12)$$

Additionally, to  $E_{ACC}$  evaluation results have been presented in terms of Mean Absolute Error ( $MAE$ ) as defined in Eq. 13.

$$MAE = \frac{1}{T} \sum_{\tau=1}^T |\hat{p}_m^\tau - p_m^\tau| \quad (13)$$

The experimental results for the eight evaluated appliances and the six experimental protocols are tabulated in Table IV for  $E_{ACC}$  values and in Table V for  $MAE$  values respectively.

TABLE IV  
ENERGY DISAGGREGATION PERFORMANCE IN TERMS OF  $E_{ACC}$  FOR DIFFERENT APPLIANCES USING DIFFERENT EXPERIMENTAL PROTOCOLS

App	I	V	V-I	$DF_H$	$DF_\Phi$	$DF_{H-\Phi}$
<b>BO</b>	80.6%	71.9%	84.9%	88.1%	88.0%	88.9%
<b>WM</b>	77.8%	65.2%	74.6%	77.9%	76.7%	79.2%
<b>KL</b>	64.6%	63.1%	65.0%	81.5%	81.1%	81.7%
<b>FR</b>	86.3%	72.4%	85.6%	88.5%	88.9%	91.2%
<b>TL</b>	78.1%	62.9%	79.5%	85.0%	84.8%	87.5%
<b>DW</b>	67.0%	62.5%	70.0%	71.4%	66.7%	75.8%
<b>MW</b>	65.7%	59.0%	70.2%	71.4%	70.5%	73.9%
<b>KT</b>	81.7%	60.9%	83.5%	86.1%	76.8%	92.5%
<b>AVG</b>	76.2%	65.2%	<b>77.3%</b>	82.0%	80.3%	<b>84.5%</b>

TABLE V  
ENERGY DISAGGREGATION PERFORMANCE IN TERMS OF  $MAE$  FOR DIFFERENT APPLIANCES USING DIFFERENT EXPERIMENTAL PROTOCOLS

App	I	V	V-I	$DF_H$	$DF_\Phi$	$DF_{H-\Phi}$
<b>BO</b>	11.86	17.18	9.23	7.28	7.34	6.79
<b>WM</b>	16.87	26.44	19.30	16.79	17.70	15.80
<b>KL</b>	21.60	22.51	21.35	11.29	11.53	11.16
<b>FR</b>	11.43	23.03	12.01	9.59	9.26	7.34
<b>TL</b>	21.76	36.87	20.37	14.91	15.11	12.42
<b>DW</b>	18.80	21.36	17.09	16.29	18.97	13.78
<b>MW</b>	16.02	19.15	13.92	13.36	13.78	12.19
<b>KT</b>	9.58	20.48	8.64	7.28	12.15	3.93
<b>Avg</b>	15.99	23.38	<b>15.24</b>	12.10	13.23	<b>10.43</b>

As can be seen in Table IV and Table V the proposed DFIA (column ' $DF_{H-\Phi}$ ') outperforms the spectrogram-based approaches ('I', 'V' and 'V-I') in all experimental protocols for all appliances and for both performance metrics. Specifically, for spectrogram-based approaches' average performance (calculated across the eight appliances) varies between 65.2-77.3% (15.24-23.38) depending on if voltage spectrograms, current spectrograms or their combination are utilized as input to the CNN. In detail, voltage spectrograms perform significantly worse comparing to current spectrograms for both  $E_{ACC}$  and  $MAE$  values. This is due to the fact that the grid voltage intrinsically does not carry much information as it is only influenced through coupling effects during the time of large current draw [44]. Combining current and voltage spectrograms has led to a performance improvement of +1.1% ( $E_{ACC}$ ) and +4.7% ( $MAE$ ) when being compared to using current spectrograms only. Furthermore, the DFIA approach (' $DF_{H-\Phi}$ ') improved NILM accuracy comparing to 'V-I' spectrograms from +3.7% (BO) up to +16.7% (KL) and the average improvement was +7.2% when considering  $E_{ACC}$  values, which is owed to its improved representation of devices through their harmonic spectrum. Moreover, when considering  $MAE$  values the improvement was found to be +26.4% (BO) up to +47.7% (KL), while the average improvement was +31.6%. It is worth mentioning that both the magnitude DFIA (' $DF_H$ ') and the phase DFIA (' $DF_\Phi$ ') setups when used separately also significantly outperform all spectrogram-based NILMs across all evaluated devices and for both performance metrics.

In a further step the proposed architecture was compared to several low-frequency and high frequency approaches from the literature that also use the UK-DALE dataset. Specifically, for comparison with high frequency approaches paper [44] was chosen, as it presents the evaluation of high frequency current and voltage spectrograms as well as their concatenation, which was adopted as baseline approach in this paper. As regards low frequency approaches, top-performing papers [56]–[58] were chosen, which are based on neural network architectures with convolutional filters as in the proposed approach, utilizing dAE in [56], seq2point/seq2seq learning in [58] and biLSTM in [57]. Furthermore, paper [59] was selected for additional comparison with approaches using source separation algo-

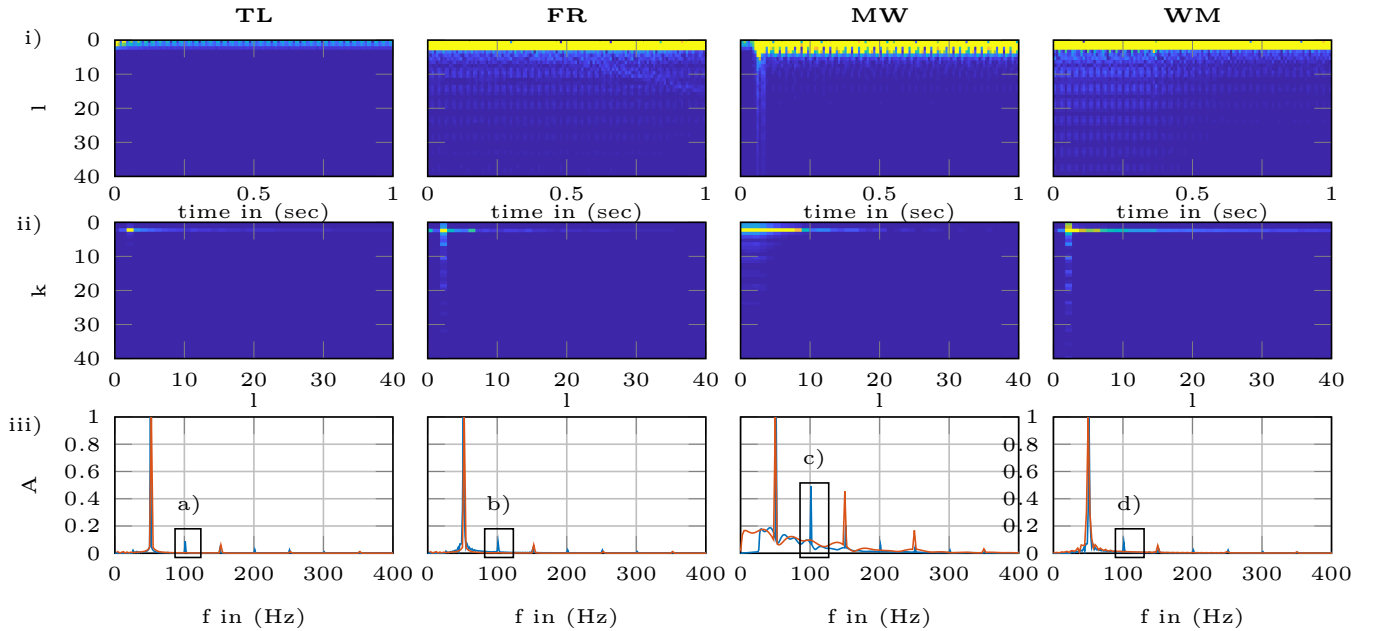


Fig. 4. Examples of current spectrograms (i), DFIA magnitudes (ii) and current harmonics (iii) of four devices (TL, FR, MW and WM), with harmonics calculated from spectrogram (red) and from DFIA (blue). Specifically, the first even order harmonic is illustrated and denoted with a), b), c) and d).

gorithms. As in these works different evaluation metrics and data splits have been used, the results from Table IV and Table V have been recalculated in terms of F1-score ( $F_1$ ) and Mean Absolute Error ( $MAE$ ).

$$F_1 = 2 \cdot \frac{TP}{2 \cdot TP + FN + FP} \quad (14)$$

where TP, FN and FP are the True Positives, False Negatives and False Positives for each identified turned on appliance combination. For the estimation of the average MAE values in the 'AVG' column of Table V, the mean value of all appliances, i.e.  $MAE = \frac{1}{M} \sum_{m=1}^M \frac{1}{T} \sum_{\tau=1}^T |\hat{p}_m^\tau - p_m^\tau|$ , was used similarly to the literature [44], [67]. Furthermore, some of the previous works do not use all appliances listed in Table IV, thus comparison is provided for the reduced set of five mutual appliances (WM, DW, FR, MW, KT). Moreover, exact comparison is not possible as these articles are using different training and testing datasets. The results in terms of F1-score and MAE are tabulated in Tables VI and VII, respectively.

TABLE VI  
ENERGY DISAGGREGATION PERFORMANCE COMPARISON IN TERMS OF  $F_1$   
IN (%) FOR DIFFERENT ARCHITECTURES

App	LF architectures				HF architectures		
	[57]	[56]	[58]	[59]	[44]	V-I	$DF_{H-\Phi}$
WM	49.0	96.0	-	84.4	80.0	90.4	95.9
DW	72.0	79.6	-	-	96.0	96.2	98.1
FR	81.0	87.9	-	76.3	96.0	95.1	97.6
MW	62.0	70.5	-	-	94.0	94.7	98.9
KT	71.0	78.3	-	94.6	97.0	97.8	99.6
AVG	67.0	<b>82.5</b>	-	<b>85.1</b>	92.6	94.8	<b>98.0</b>

TABLE VII  
ENERGY DISAGGREGATION PERFORMANCE COMPARISON IN TERMS OF  
MAE IN (WATTS) FOR DIFFERENT ARCHITECTURES

App	LF architectures				HF architectures		
	[57]	[56]	[58]	[59]	[44]	V-I	$DF_{H-\Phi}$
WM	11.0	-	12.7	-	1.4	3.4	2.2
DW	30.0	-	27.7	-	5.8	4.7	1.6
FR	18.0	-	20.8	-	5.9	8.5	2.6
MW	6.0	-	8.7	-	0.9	6.2	3.5
KT	7.0	-	7.4	-	3.9	4.1	2.9
AVG	14.4	-	15.5	-	3.6	5.4	<b>2.6</b>

As can be seen in Tables VI and VII the LF architectures generally perform worse than the HF ones. Specifically, the approach in [56] utilizing dAEs with performance equal to 82.5% in terms of F1-score is outperformed by more than 10% by approaches based on HF like [44]. Similarly, biLSTM proposed in [57] having the best performance among the LF architectures when using MAE as performance metric is significantly outperformed by [44] using concatenated CNNs. The proposed DFIA approach further improves the performance, significantly outperforming LF architectures and improving the performance of the concatenated CNN architecture of [44] by 5.4% for F1-scores (98.0%) and reducing the MAE by 1.0.

## VI. DISCUSSION

Further to the experimental results presented in Section V analysis of the underlying advantages of the proposed DFIA compared to spectrograms was performed. The characteristic device signatures represented by DFIA for four appliances are presented in Subsection VI-A, three case studies of energy disaggregation performance are analyzed in Subsection VI-B

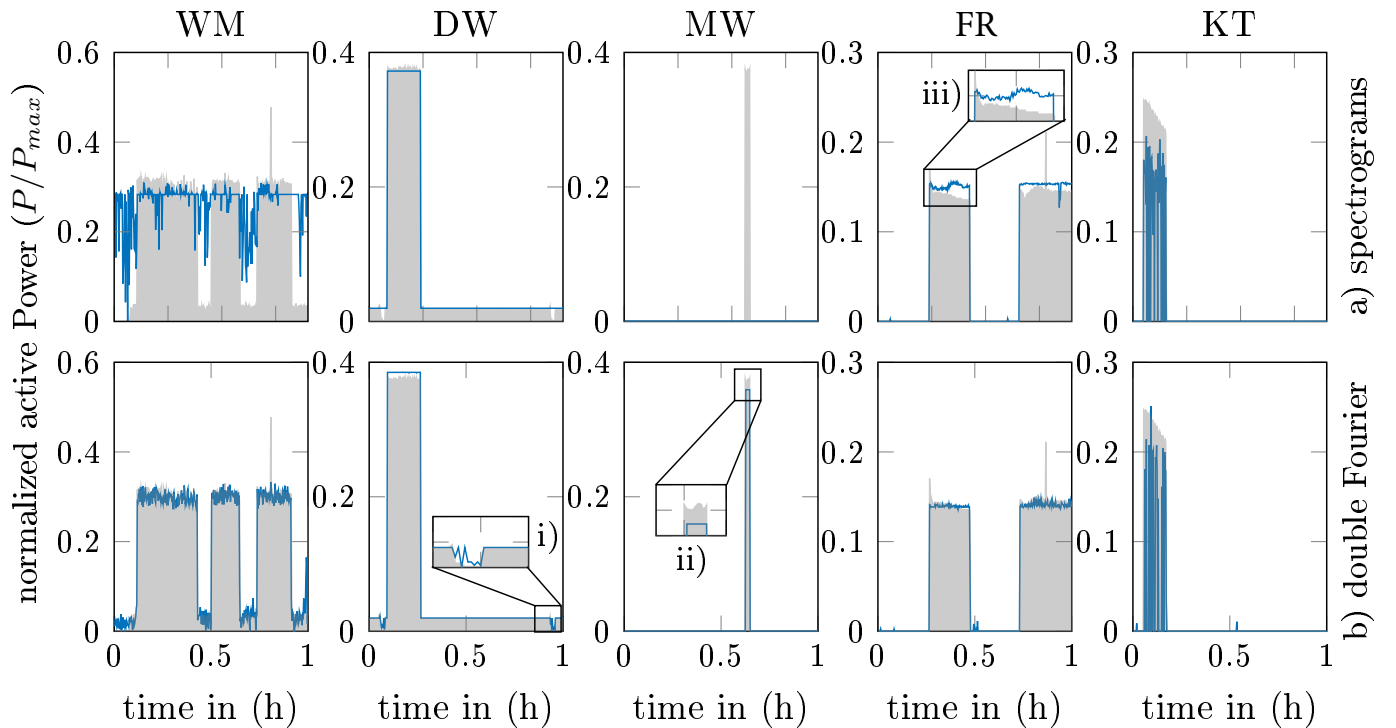


Fig. 5. Examples of active power estimation (blue line) of five devices for one hour for (a) spectrogram-based analysis and (b) double Fourier integral analysis

and computational processing execution time measurements are provided in Subsection VI-C.

#### A. Spectrogram vs. DFIA Signatures

As shown in Eq. 3 except the fundamental component and baseband harmonics (i.e. the current harmonics) and the carrier harmonics (i.e. voltage harmonics) which exist in the corresponding spectrograms, the additional information that DFIA offers is the sideband harmonics. In Fig. 4 the magnitudes of the spectrograms and DFIA as well as the current harmonics of four devices are shown.

As shown in Fig. 4, the DFIA magnitude of each device has a pattern which visually is more distinctive than the corresponding one of the current spectrogram (e.g. FR and WM spectrograms are quite similar). In detail, this has resulted to 7.2% of average improvement in NILM accuracy as shown in Table IV. Calculating the corresponding current harmonics, it can be seen that the spectrogram-based harmonics include only the odd ones (i.e. 1st, 3rd, 5th, etc.), as found in the current signal. Conversely the DFIA-based approach considers interaction of current and voltage giving a complete representation of the spectral content of the device with frequencies to be found at  $f = f_{el}k + f_{el}l$  with  $1 \leq k < K$  and  $1 \leq l < L$  being index variables of voltage and current as described in Eq. 3. In this context especially the presence of the even order harmonics in the FFT signals have to be pointed out, which are only captured by DFIA and not by the spectrogram analysis.

#### B. Energy Disaggregation Case Studies

To compare and contrast the spectrogram-based analysis with the proposed DFIA method in terms of their ability

to detect transient and steady-state patterns in appliances' signatures, detailed examination of estimation signals was performed. In Fig. 5 examples of the active power estimation of five devices for a time window of one hour for the baseline spectrogram-based analysis (V-I) and for the proposed DFIA ( $DF_{H-\Phi}$ ) are illustrated in blue, while the ground truth active power of each device is shown in gray. In the same figure, three characteristic cases, denoted as '(i)' in DW '(ii)' in MW and '(iii)' in FR, are shown in bounding boxes and are analyzed below.

In specific, the first case denoted as '(i)' in DW device is a small drop (signal trough) with duration of approximately 2 minutes and trough depth of 0.02 (normalized). As can be seen, the spectrogram-based approach cannot track this small trough in contrast to DFIA which detects it. The second case denoted as '(ii)' in the MW device is a very short-duration peak in the active power (in the order of 46s seconds with amplitude increase of 0.35 (normalized)), which is not detected by the spectrogram-based method and maybe can be assigned to other appliances with longer working routines and the same/similar active power amplitude, like the WM in the example shown in Fig. 5. Both examples '(i)' and '(ii)' demonstrate the advantage of the proposed DFIA in detecting narrow crests and troughs in the signal, which in general cannot be detected by the spectrogram-based method. The third case denoted as '(iii)' in the FR device is a signal decay pattern which was not estimated accurately from the spectrogram-based method but instead estimates a divergent amplitude waveform, in contrast to DFIA which models this decay pattern relatively well. To further analyse this behaviour, we 'zoomed in' the normalized transient period (i.e. the start-

up of FR device) shown in the bounding box of Fig. 6a and the corresponding high-frequency transient normalized current at the same time interval (transient period) shown in Fig. 6b.

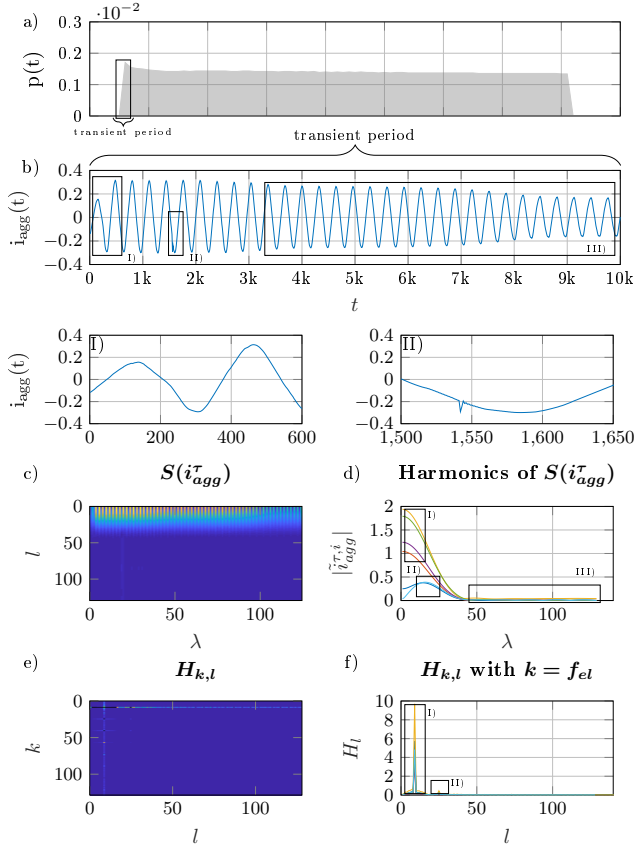


Fig. 6. High-frequency analysis of transient period of a fridge start-up: (a) active power of the fridge, (b) transient aggregated current, (c) magnitude of selected current harmonics per time frame, (d) current spectrogram, (e) magnitude of selected DFIA harmonics for  $k = f_{el}$ , and (f) DFIA magnitude. Each harmonic is illustrated with a unique color with descending order: 1<sup>st</sup>: blue, 2<sup>nd</sup>: orange, 3<sup>rd</sup>: yellow, 4<sup>th</sup>: purple, 5<sup>th</sup>: green, 6<sup>th</sup>: light blue.

As shown in Fig. 6b, in the transient current of the fridge three regions of interest have been identified, namely region ‘I’ which corresponds to the beginning of the transient period, region ‘II’ which contains a trough distortion (maybe caused by the switching of another appliance) and region ‘III’ which is the decay of the fridge’s transient period. To investigate how DFIA and spectrogram-based methods capture these micro-events the corresponding current harmonics were calculated in each case. For visualization purposes 6 harmonics above the fundamental frequency, evenly spaced up to the maximum frequency, are chosen. Specifically, the current spectrogram is shown in Fig. 6c and from the corresponding current harmonics of it, as shown in Fig. 6d, it is observed that while most harmonics decrease in time starting from a peak some of them present a peak delay which is most probably responsible for the inability of the regression estimation in Fig. 5a-FR to follow the decay. In contrast to current spectrogram, in DFIA the current harmonics (estimated for voltage frequency  $k=f_{el}$  with  $f_{el}=50$  Hz) that correspond to the trough distortion (II) have magnitude much lower than the rest harmonics thus practically not causing significant errors in device’s power

consumption estimation in Fig. 5b-FR.

### C. Realtime Capability

The proposed architecture clearly aims to improve the performance of the NILM architecture, but as high-frequency approaches are computational expensive real-time capability must be considered. Therefore, we calculated the execution time per sample for V-I spectrograms and  $DF_{H-\Phi}$  on an Intel i7 7700k CPU with 64GB RAM using two Nvidia GTX 1080Ti in SLI mode. The Average Execution Time (AET) per sample, when using GPU calculations, is compared to the HF approach of [44], which was calculated on the same GPU hardware and Tensorflow. The results are shown in Table VIII.

TABLE VIII  
COMPARISON OF AVERAGE EXECUTION TIME (AET) FOR  
DISAGGREGATING ONE SAMPLE OF AGGREGATED DATA.

Approach	V-I	$DF_{H-\Phi}$	[44]
AET (ms)	18	221	69

As illustrated in Table VIII the average execution time of the proposed DFIA approach is approximately 3 times larger than the AET of [44]. However, considering its real-time capability the proposed approach is still significantly lower than real-time with one sample (1 second due to device signals being monitored at 1 Hz) of the ground-truth signal being disaggregated in 221ms.

## VII. CONCLUSION

In this paper the use of double Fourier integral analysis for high frequency energy disaggregation was proposed. Specifically, raw aggregated current and voltage waveforms are transformed to their two-dimensional frequency representation and used to train a Convolutional Neural Network for regression. The proposed methodology was evaluated on the UK-DALE database improving performance by 7.2% when compared to current and voltage spectrograms, and 5.4% when compared to previously published CNN-based architectures. Detailed analysis of the energy disaggregation performance of devices like washing machine, microwave, lights and fridge showed the advantageous ability of double Fourier integral based representation to capture signature patterns with very short duration as well as to contain all current and voltage harmonics including sideband harmonics, influenced by interaction of current and voltage. Based on the promising results of the DFIA the following three topics should be investigated in future research. First, investigation of the transferability capability is needed, in order to examine if DFIA can be used in the case of pre-training device models. Second, even though the full sampling resolution of 16 kHz was used in the proposed approach an investigation on the effect of different sampling rates will reveal the minimum needed sampling frequency to retain high NILM accuracy while reducing storage and computational cost. Third, considering the temporal characteristics of the NILM problem investigation of a LSTM-CNN based architecture with additional optimization of the subframe-length might be beneficial for capturing temporal information (high-frequency ground-truth data).

## REFERENCES

- [1] L. Pérez-Lombard, J. Ortiz, and C. Pout, "A review on buildings energy consumption information," *Energy and Buildings*, vol. 40, no. 3, pp. 394–398, 2008.
- [2] K. R. K. L. L. H. A. A. L. Peter Lusis, "Short-term residential load forecasting: Impact of calendar effects and forecast granularity," *Applied Energy*, vol. 205, pp. 654–669, 2017.
- [3] S. Welikala, C. Dinesh, M. P. B. Ekanayake, R. I. Godaliyadda, and J. Ekanayake, "Incorporating appliance usage patterns for non-intrusive load monitoring and load forecasting," *IEEE Transactions on Smart Grid*, vol. 10, no. 1, pp. 448–461, 2019.
- [4] B. Rajasekhar, N. Pindoriya, W. Tushar, and C. Yuen, "Collaborative energy management for a residential community: a non-cooperative and evolutionary approach," *IEEE Transactions on Emerging Topics in Computational Intelligence*, vol. 3, no. 3, pp. 177–192, 2019.
- [5] Y. Hong, D. Xu, W. Yang, B. Jiang, and X.-G. Yan, "A novel multi-agent model-free control for state-of-charge balancing between distributed battery energy storage systems," *IEEE Transactions on Emerging Topics in Computational Intelligence*, 2020.
- [6] B. Rajasekhar, W. Tushar, C. Lork, Y. Zhou, C. Yuen, N. M. Pindoriya, and K. L. Wood, "A survey of computational intelligence techniques for air-conditioners energy management," *IEEE Transactions on Emerging Topics in Computational Intelligence*, 2020.
- [7] C. Ogwumike, M. Short, and M. Denai, "Near-optimal scheduling of residential smart home appliances using heuristic approach," in *IEEE International Conference on Industrial Technology (ICIT), 2015*. Piscataway, NJ: IEEE, 2015, pp. 3128–3133.
- [8] J. Kelly and W. Knottenbelt, "Does disaggregated electricity feedback reduce domestic electricity consumption? a systematic review of the literature," 3rd International NILM Workshop. [Online]. Available: <http://arxiv.org/pdf/1605.00962v2>
- [9] H. Kim, M. Marwah, M. Arlitt, G. Lyon, and J. Han, "Unsupervised disaggregation of low frequency power measurements," in *Proceedings of the 2011 SIAM International Conference on Data Mining*, [Philadelphia, PA], 2011, pp. 747–758.
- [10] K. D. Anderson, M. E. Berges, A. Oceau, D. Benitez, and J. M. Moura, "Event detection for non intrusive load monitoring," in *IECON 2012*. Piscataway, NJ: IEEE, 2012, pp. 3312–3317.
- [11] G. W. Hart, "Nonintrusive appliance load monitoring," *Proceedings of the IEEE*, vol. 80, no. 12, pp. 1870–1891, 1992.
- [12] A. Harell, S. Makonin, and I. V. Bajić, "Wavenilm: A causal neural network for power disaggregation from the complex power signal," 2019. [Online]. Available: <https://arxiv.org/pdf/1902.08736>
- [13] M. DrIncecco, S. Squartini, and M. Zhong, "Transfer learning for non-intrusive load monitoring," *IEEE Transactions on Smart Grid*, p. 1, 2019.
- [14] P. A. Schirmer and I. Mporas, "Energy disaggregation using fractional calculus," in *ICASSP 2020 - 2020 IEEE International Conference on Acoustics, Speech and Signal Processing (ICASSP)*. IEEE, 2020, pp. 3257–3261.
- [15] M. Kaselimi, N. Doulamis, A. Doulamis, A. Voulodimos, and E. Protopapadakis, "Bayesian-optimized bidirectional lstm regression model for non-intrusive load monitoring," in *ICASSP 2019 - 2019 IEEE International Conference on Acoustics, Speech and Signal Processing (ICASSP)*. IEEE, 2019, pp. 2747–2751.
- [16] L. Mauch and B. Yang, "A new approach for supervised power disaggregation by using a deep recurrent lstm network," in *2015 IEEE Global Conference on Signal and Information Processing (GlobalSIP)*. Piscataway, NJ and Piscataway, NJ: IEEE, 2015, pp. 63–67.
- [17] S. Makonin, F. Popowich, I. V. Bajic, B. Gill, and L. Bartram, "Exploiting hmm sparsity to perform online real-time nonintrusive load monitoring," *IEEE Transactions on Smart Grid*, vol. 7, no. 6, pp. 2575–2585, 2016.
- [18] J. Z. Kolter and T. Jaakkola, "Approximate inference in additive factorial hmms with application to energy disaggregation," in *Proceedings of the Fifteenth International Conference on Artificial Intelligence and Statistics*, ser. Proceedings of Machine Learning Research, N. D. Lawrence and M. Girolami, Eds., vol. 22. La Palma, Canary Islands: PMLR, 2012, pp. 1472–1482. [Online]. Available: <http://proceedings.mlr.press/v22/zico12.html>
- [19] K. Basu, V. Debusschere, S. Bacha, U. Maulik, and S. Bondyopadhyay, "Nonintrusive load monitoring: A temporal multilabel classification approach," *IEEE Transactions on Industrial Informatics*, vol. 11, no. 1, pp. 262–270, 2015.
- [20] P. A. Schirmer, I. Mporas, and A. Sheikh-Akbari, "Robust energy disaggregation using appliance-specific temporal contextual information," *EURASIP Journal on Advances in Signal Processing*, vol. 2020, no. 1, p. 394, 2020.
- [21] S. Henriët, U. Simsekli, S. D. Santos, B. Fuentes, and G. Richard, "Independent-variation matrix factorization with application to energy disaggregation," *IEEE Signal Processing Letters*, vol. 26, no. 11, pp. 1643–1647, 2019.
- [22] M. Figueiredo, B. Ribeiro, and A. de Almeida, "Electrical signal source separation via nonnegative tensor factorization using on site measurements in a smart home," *IEEE Transactions on Instrumentation and Measurement*, vol. 63, no. 2, pp. 364–373, 2014.
- [23] A. Rahimpour, H. Qi, D. Fugate, and T. Kuruganti, "Non-intrusive energy disaggregation using non-negative matrix factorization with sum-to-k constraint," *IEEE Transactions on Power Systems*, vol. 32, no. 6, pp. 4430–4441, 2017.
- [24] S. Zeinal-Kheiri, A. M. Shotorbani, and B. Mohammadi-Ivatloo, "Residential load disaggregation considering state transitions," *IEEE Transactions on Industrial Informatics*, vol. 16, no. 2, pp. 743–753, 2020.
- [25] S. Singh and A. Majumdar, "Analysis co-sparse coding for energy disaggregation," *IEEE Transactions on Smart Grid*, p. 1, 2017.
- [26] —, "Deep sparse coding for non-intrusive load monitoring," *IEEE Transactions on Smart Grid*, p. 1, 2017.
- [27] R. Machlev, Y. Levron, and Y. Beck, "Modified cross-entropy method for classification of events in nilm systems," *IEEE Transactions on Smart Grid*, vol. 10, no. 5, pp. 4962–4973, 2019.
- [28] N. Pathak, N. Roy, and A. Biswas, "Iterative signal separation assisted energy disaggregation," in *2015 Sixth International Green and Sustainable Computing Conference*. Piscataway, NJ: IEEE, 2015, pp. 1–8.
- [29] K. He, L. Stankovic, J. Liao, and V. Stankovic, "Non-intrusive load disaggregation using graph signal processing," *IEEE Transactions on Smart Grid*, p. 1, 2016.
- [30] P. A. Schirmer, I. Mporas, and M. Paraskevas, "Energy disaggregation using elastic matching algorithms," *Entropy*, vol. 22, no. 1, p. 71, 2020.
- [31] P. A. Schirmer and I. Mporas, "Statistical and electrical features evaluation for electrical appliances energy disaggregation," *Sustainability*, vol. 11, no. 11, p. 3222, 2019.
- [32] A. S. Bouhouras, P. A. Gkaidatzis, E. Panagiotou, N. Poulakis, and G. C. Christoforidis, "A nilm algorithm with enhanced disaggregation scheme under harmonic current vectors," *Energy and Buildings*, vol. 183, pp. 392–407, 2019.
- [33] N. Sadeghianpourhamami, J. Ruysinck, D. Deschrijver, T. Dhaene, and C. Develder, "Comprehensive feature selection for appliance classification in nilm," *Energy and Buildings*, vol. 151, pp. 98–106, 2017.
- [34] R. Machlev, D. Tolkachov, Y. Levron, and Y. Beck, "Dimension reduction for nilm classification based on principle component analysis," *Electric Power Systems Research*, vol. 187, p. 106459, 2020.
- [35] C. Dinesh, B. W. Nettasinghe, R. I. Godaliyadda, M. P. B. Ekanayake, J. Ekanayake, and J. V. Wijayakulasooriya, "Residential appliance identification based on spectral information of low frequency smart meter measurements," *IEEE Transactions on Smart Grid*, vol. 7, no. 6, pp. 2781–2792, 2016.
- [36] P. Bilski and W. Winiecki, "The rule-based method for the non-intrusive electrical appliances identification," in *IDAACS'2015*. Piscataway, NJ: IEEE, 2015, pp. 220–225.
- [37] D. H. Green, S. R. Shaw, P. Lindahl, T. J. Kane, J. S. Donnal, and S. B. Leeb, "A multiscale framework for nonintrusive load identification," *IEEE Transactions on Industrial Informatics*, vol. 16, no. 2, pp. 992–1002, 2020.
- [38] A. Aboulian, D. H. Green, J. F. Switzer, T. J. Kane, G. V. Bredariol, P. Lindahl, J. S. Donnal, and S. B. Leeb, "Nilm dashboard: A power system monitor for electromechanical equipment diagnostics," *IEEE Transactions on Industrial Informatics*, vol. 15, no. 3, pp. 1405–1414, 2019.
- [39] A. Wójcik, W. Winiecki, R. Łukaszewski, and P. Bilski, "Analysis of transient state signatures in electrical household appliances," in *2019 10th IEEE International Conference on Intelligent Data Acquisition and Advanced Computing Systems: Technology and Applications (IDAACS)*, vol. 2. IEEE, 2019, pp. 639–644.
- [40] J. M. Gillis, S. M. Alshareef, and W. G. Morsi, "Nonintrusive load monitoring using wavelet design and machine learning," *IEEE Transactions on Smart Grid*, vol. 7, no. 1, pp. 320–328, 2016.
- [41] J. M. Gillis and W. G. Morsi, "Non-intrusive load monitoring using semi-supervised machine learning and wavelet design," *IEEE Transactions on Smart Grid*, vol. 8, no. 6, pp. 2648–2655, 2017.
- [42] Y. Liu, X. Wang, and W. You, "Non-intrusive load monitoring by voltage-current trajectory enabled transfer learning," *IEEE Transactions on Smart Grid*, vol. 10, no. 5, pp. 5609–5619, 2019.

- [43] H. Lange and M. Bergés, “Bolt: Energy disaggregation by online binary matrix factorization of current waveforms,” in *Proceedings of the 3rd ACM International Conference on Systems for Energy-Efficient Built Environments*, 2016, pp. 11–20.
- [44] Q. Wu and F. Wang, “Concatenate convolutional neural networks for non-intrusive load monitoring across complex background,” *Energies*, vol. 12, no. 8, p. 1572, 2019.
- [45] H.-H. Chang, K.-L. Lian, Y.-C. Su, and W.-J. Lee, “Power-spectrum-based wavelet transform for nonintrusive demand monitoring and load identification,” *IEEE Transactions on Industry Applications*, vol. 50, no. 3, pp. 2081–2089, 2014.
- [46] T. Hassan, F. Javed, and N. Arshad, “An empirical investigation of  $v$ - $i$  trajectory based load signatures for non-intrusive load monitoring,” *IEEE Transactions on Smart Grid*, vol. 5, no. 2, pp. 870–878, 2014.
- [47] W. Wichakool, Z. Remscrim, U. A. Orji, and S. B. Leeb, “Smart metering of variable power loads,” *IEEE Transactions on Smart Grid*, vol. 6, no. 1, pp. 189–198, 2015.
- [48] W. Wichakool, A.-T. Avestruz, R. W. Cox, and S. B. Leeb, “Modeling and estimating current harmonics of variable electronic loads,” *IEEE Transactions on Power Electronics*, vol. 24, no. 12, pp. 2803–2811, 2009.
- [49] P. Held, S. Mauch, A. Saleh, D. Ould Abdeslam, and D. Benyoucef, “Frequency invariant transformation of periodic signals (fit-ps) for classification in nilm,” *IEEE Transactions on Smart Grid*, vol. 10, no. 5, pp. 5556–5563, 2019.
- [50] H. Liu, Q. Zou, and Z. Zhang, “Energy disaggregation of appliances consumptions using ham approach,” *IEEE Access*, vol. 7, pp. 185 977–185 990, 2019.
- [51] J. Froehlich, E. Larson, S. Gupta, G. Cohn, M. Reynolds, and S. Patel, “Disaggregated end-use energy sensing for the smart grid,” *IEEE Pervasive Computing*, vol. 10, no. 1, pp. 28–39, 2011.
- [52] S. R. Bowes, “New sinusoidal pulsewidth-modulated inverter,” in *Proceedings of the Institution of Electrical Engineers*, vol. 122, no. 11. IET, 1975, pp. 1279–1285.
- [53] S. Bowes and B. Bird, “Novel approach to the analysis and synthesis of modulation processes in power converters,” in *Proceedings of the Institution of Electrical Engineers*, vol. 122, no. 5. IET, 1975, pp. 507–513.
- [54] W. Bennett, “New results in the calculation of modulation products,” *The Bell System Technical Journal*, vol. 12, no. 2, pp. 228–243, 1933.
- [55] H. S. Black, *Modulation theory*. van Nostrand, 1953.
- [56] K. S. Barsim and B. Yang, “On the feasibility of generic deep disaggregation for single-load extraction.” [Online]. Available: <https://arxiv.org/pdf/1802.02139>
- [57] J. Kelly and W. Knottenbelt, “Neural nilm,” in *BuildSys’15*, D. Culler, Y. Agarwal, and R. Mangharam, Eds. New York, New York: The Association for Computing Machinery, 2015, pp. 55–64.
- [58] C. Zhang, M. Zhong, Z. Wang, N. Goddard, and C. Sutton, “Sequence-to-point learning with neural networks for nonintrusive load monitoring.” [Online]. Available: <http://arxiv.org/pdf/1612.09106v3>
- [59] S. Pandey and G. Karypis, “Structured dictionary learning for energy disaggregation,” in *E-Energy ’19*, Unknown, Ed. New York, New York: The Association for Computing Machinery, 2019, pp. 24–34.
- [60] D. Yildirim and E. Fuchs, “Commentary on various formulations of distortion power  $d$ ,” *IEEE Power Engineering Review*, vol. 19, no. 5, pp. 50–52, 1999.
- [61] D. G. Holmes and T. A. Lipo, *Pulse width modulation for power converters: Principles and practice / D. Grahame Holmes, Thomas A. Lipo*. Hoboken, N.J. and Great Britain: John Wiley, 2003. [Online]. Available: <http://www.loc.gov/catdir/description/wiley037/2003057626.html>
- [62] R. Wang, J. Zhao, and Y. Liu, “A comprehensive investigation of four-switch three-phase voltage source inverter based on double fourier integral analysis,” *IEEE Transactions on Power Electronics*, vol. 26, no. 10, pp. 2774–2787, 2011.
- [63] J. Z. Kolter and M. J. Johnson, Eds., *REDD: A Public Data Set for Energy Disaggregation Research*, 2011.
- [64] J. Kelly and W. Knottenbelt, “The uk-dale dataset, domestic appliance-level electricity demand and whole-house demand from five uk homes,” *Scientific data*, vol. 2, p. 150007, 2015.
- [65] T. Kriebchaumer and H.-A. Jacobsen, “Blond, a building-level office environment dataset of typical electrical appliances,” *Scientific data*, vol. 5, p. 180048. [Online]. Available: <https://www.nature.com/articles/sdata201848.pdf>
- [66] A. O. D. B. D. C. A. R. K. Anderson and M. Berges, Eds., *BLUED: A Fully Labeled Public Dataset for Event-Based Non-Intrusive Load Monitoring Research*, pages 12–16, 2012.
- [67] Y. Pan, K. Liu, Z. Shen, X. Cai, and Z. Jia, “Sequence-to-subsequence learning with conditional gan for power disaggregation,” in *ICASSP 2020 - 2020 IEEE International Conference on Acoustics, Speech and Signal Processing (ICASSP)*, 2020, pp. 3202–3206.



**Pascal A. Schirmer** received the B.Eng. degree in electrical engineering from the University of Applied Sciences, Esslingen, Germany, in 2018 and the Ph.D. in electrical engineering from the University of Hertfordshire, UK, in 2021. Since 2021 he works for the R&D department for the development of power electronics at BMW AG, Munich, Germany, where he is responsible for the lifetime evaluation of power electronic systems. Furthermore, he is a visiting research fellow at the University of Hertfordshire, UK, and a visiting lecturer for electro-mobility at the TAE, Esslingen, Germany. Moreover, his research interests include energy disaggregation and power electronics.



**Iosif Mporas** is Senior Lecturer in Information Engineering at the University of Hertfordshire UK, since 2016. He holds a Diploma (5-years degree, 2004) in Electrical and Computer Engineering from the University of Patras, Greece and a PhD degree (2009) from the same University. From 2010 until 2016 he was Adjunct Assistant Professor at Technological Educational Institute of Western Greece. Also, from 2009 until 2016 he was postdoctoral researcher at the University of Patras. He has participated in more than 10 EU-funded R&D projects as researcher, senior researcher and as Principal Investigator. His research interests are in applications of signal processing and machine learning. He serves as reviewer of grant applications, as reviewer of international journals and as Programme Committee member in international conferences, while he was the General Chair of the joint SPECOM/ICR 2017 conference and the Technical Chair of the ICESF 2020 conference. He has published more than 100 articles in international journals and conferences cited more than 1000 times.